

# Nucleation and Bulk Crystallization in Binary Phase Field Theory

László Gránásy,<sup>1</sup> Tamás Börzsönyi,<sup>1,2</sup> and Tamás Pusztai<sup>1</sup>

<sup>1</sup>*Research Institute for Solid State Physics and Optics, POB 49, H-1525 Budapest, Hungary*

<sup>2</sup>*Groupe de Physique des Solides, CNRS UMR 75-88, Universités Paris*

*VI at VII, Tour 23, 2 place Jussieu, 75251 Paris Cedex 05, France*

(Dated: October 22, 2018)

We present a phase field theory for binary crystal nucleation. In the one-component limit, quantitative agreement is achieved with computer simulations (Lennard-Jones system) and experiments (ice-water system) using model parameters evaluated from the free energy and thickness of the interface. The critical undercoolings predicted for Cu–Ni alloys accord with the measurements, and indicate homogeneous nucleation. The Kolmogorov exponents deduced for dendritic solidification and for “soft-impingement” of particles via diffusion fields are consistent with experiment.

PACS numbers: 81.10.Aj, 82.60.Nh, 64.60.Qb

Understanding alloy solidification is of vast practical and theoretical importance. While the directional geometry in which the solidification front propagates from a cool surface towards the interior of a hot melt is understood fairly well, less is known of equiaxial solidification that takes place in the interior of the melt. The latter plays a central role in processes such as alloy casting, hibernation of biological tissues, hail formation, and crystallization of proteins and glasses. The least understood stage of these processes is nucleation, during which seeds of the crystalline phase appear via thermal fluctuations. Since the physical interface thickness is comparable to the typical size of critical fluctuations that are able to grow to macroscopic sizes, these fluctuations are nearly all interface. Accordingly, the diffuse interface models lead to a considerably more accurate description of nucleation than those based on a sharp interface [1, 2].

The phase field theory, a recent diffuse interface approach, emerged as a powerful tool for describing complex solidification patterns such as dendritic, eutectic, and peritectic growth morphologies [3]. It is of interest to extend this model to nucleation and post-nucleation growth including diffusion controlled “soft-impingement” of growing crystalline particles, expected to be responsible for the unusual transformation kinetics recently seen during the formation of nanocrystalline materials [4].

In this Letter, we develop a phase field theory for crystal nucleation and growth, and apply it to current problems of unary and binary equiaxial solidification.

Our starting point is the free energy functional

$$F = \int d\mathbf{r} \left\{ \frac{\epsilon^2 T}{2} (\nabla \phi)^2 + f(\phi, c) \right\}, \quad (1)$$

developed along the lines described in [5, 6]. Here  $\phi$  and  $c$  are the phase and concentration fields,  $f(\phi, c) = WTg(\phi) + [1 - P(\phi)]f_S + P(\phi)f_L$  is the local free energy density,  $W = (1 - c)W_A + cW_B$  the free energy scale, the quartic function  $g(\phi) = \phi^2(1 - \phi)^2/4$  that emerges from density functional theory [7] ensures the double-well form of  $f$ , while the function  $P(\phi) = \phi^3(10 - 15\phi +$

$6\phi^2)$  switches on and off the solid and liquid contributions  $f_{S,L}$ , taken from the ideal solution model. (A and B refer to the constituents.)

For binary alloys the model contains three parameters  $\epsilon$ ,  $W_A$  and  $W_B$  that reduce to two ( $\epsilon$  and  $W$ ) in the one-component limit. They can be fixed if the respective interface free energy  $\gamma$ , melting point  $T_f$ , and interface thickness  $\delta$  are known [8]. Such information is available for the Lennard-Jones, ice-water, and Cu–Ni systems [9], offering a quantitative test of our approach.

Relying on the isothermal approximation the time evolution is described by Langevin equations  $\partial\phi/\partial t = -M_\phi(\delta F/\delta\phi) + \zeta_\phi$  and  $\partial c/\partial t = \nabla[M_c \nabla(\delta F/\delta c)] + \zeta_{\nabla c}$ , where  $(\delta F/\delta x)$  stands for the functional derivatives ( $x = \phi, c$ ),  $M_x$  are mobilities, while  $\zeta_\phi$  and  $\zeta_{\nabla c}$  are appropriate noises added to RHS to mimic thermal fluctuations. The dimensionless form of these equations [10] is obtained by measuring length and time in units  $\xi$  and  $\xi^2/D_L$ ,  $t = \tilde{t}\xi^2/D_L$ ,  $\mathbf{r} = \tilde{\mathbf{r}}/\xi$ . Here  $\xi$  and  $D_L$  are the characteristic length scale and the diffusion coefficient in the liquid, while the quantities with tilde are dimensionless.

The critical fluctuation (nucleus) is a non-trivial time-independent solution of the governing equations. For spherical symmetry (a reasonable assumption), the phase field equation reduces to  $\nabla^2\phi = \Delta\mu(\phi, c)/(\epsilon^2 T)$ . Here  $\Delta\mu(\phi, c) = WTg'(\phi) + [(1 - c)\Delta f_A + c\Delta f_B]P'(\phi)$  is the local chemical potential difference relative to the initial liquid, prime stands for differentiation with respect to the argument, the local concentration is related to the phase-field as  $c(\phi) = c_\infty e^{-y}/(1 - c_\infty + c_\infty e^{-y})$ , where  $y = v(W_B - W_A)g(\phi)/R + v(\Delta f_B - \Delta f_A)[P(\phi) - 1]/RT$ , while  $\Delta f_i$  are the volumetric free energy differences between the pure liquid and solid phases. Solving these equations numerically under boundary conditions that prescribe bulk liquid properties far from the fluctuations ( $\phi \rightarrow 1$ , and  $c \rightarrow c_\infty$  for  $r \rightarrow \infty$ ), and zero field-gradients at the center, one obtains the free energy of critical fluctuation as  $W^* = F - F_0$ . Here  $F$  is obtained by numerically evaluating Eq. (1) after having the time-independent solutions inserted, while  $F_0$  is the free energy of the initial

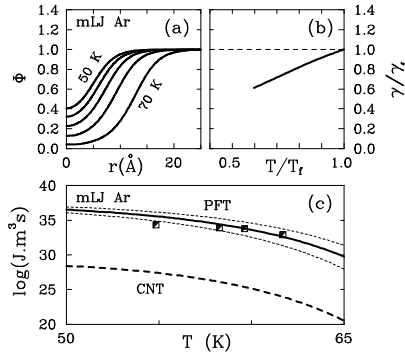


FIG. 1: Nucleation in the modified Lennard-Jones system: (a) Radial phase field profiles for critical fluctuations at several temperatures. (b) Relative interfacial free energy vs. reduced temperature. (c) Comparison of nucleation rates predicted by the phase field theory (PFT), the classical sharp interface theory (CNT) and computer simulations (squares) [15]. Short-dashed lines show the limits of nucleation rate allowed by the error of the interfacial free energy.  $\epsilon = 137.07\text{k}$  and  $\sigma = 3.383 \text{\AA}$  are taken for Ar. Below 61.7 K, the simulations increasingly underestimate the true nucleation rate due to an unknown equilibration period caused by quenching the liquid to the nucleation temperature [15].

liquid. This is compared with  $W^* = (16\pi/3)\gamma_f^3/\Delta f^2$  from the sharp interface “droplet” model of the classical nucleation theory [11], where  $\gamma_f = \gamma(T_f)$ .

The homogeneous nucleation rate is calculated as  $J = J_0 \exp\{-W^*/kT\}$ , where the nucleation prefactor  $J_0$  of the classical kinetic approach is used [12], which proved consistent with experiments [11].

To study the soft-impingement problem we introduce a non-conservative orientation field  $\theta$ , which is random in the liquid, and has a constant value between 0 and 1 in the crystal that determines crystal orientation in the laboratory frame. By this, we capture the feature that the short-range order in the solid and liquid are usually similar, with the obvious difference that the building units have a uniform orientation in the crystal, while their orientation fluctuates in the liquid. Following [13], we assume that the grain boundary energy acts in the solid and is proportional to  $|\nabla\theta|$ . We realize this by adding  $f_{ori} = \mathcal{M}|\nabla\theta|$  to  $f_S$ , where coefficient  $\mathcal{M}$  is assumed to be independent of  $c$ . The respective equation of motion has the form  $\partial\theta/\partial t = -M_\theta(\delta F/\delta\theta) + \zeta_\theta$ , yielding

$$\frac{\partial\theta}{\partial t} = \frac{\xi M_\theta \mathcal{M}}{D_L} \tilde{\nabla} \left\{ [1 - P(\phi)] \frac{\tilde{\nabla}\theta}{|\tilde{\nabla}\theta|} \right\} + \zeta_\theta, \quad (2)$$

where  $\zeta_\theta = \zeta_{\theta,0}P(\phi)$ , and  $M_\theta = M_{\theta,S} + P(\phi)(M_{\theta,L} - M_{\theta,S})$ , while subscripts S and L indicate the values for the bulk liquid and solid phases. When  $\phi < 1$ , Eq. (2) switches in orientational ordering, and chooses the value of  $\theta$  that survives as the orientation of the particle,

which then serves as the direction relative to which the anisotropy of  $\gamma$  ( $= \gamma_0 \{1 + s_0 \cos[m(\vartheta - \theta)]\}$  for  $m$ -fold symmetry) is measured. A similar model has been successfully applied for describing grain boundary dynamics [13, 14]. Unlike previous work, in our approach the orientation field  $\theta$  is coupled to the phase field, and extends to the liquid phase where crystallographic orientation develops from orientational fluctuations. While our model incorporates grain boundary dynamics, our primary interest is solidification, and  $M_{\theta,S}$  is set so that grain rotation is negligible on the time scale of solidification.

Nucleation is incorporated into the simulations as follows. Method I.: By including white noise into the governing equations of amplitude that forces nucleation in the spatial and time windows used. Method II.: The simulation area is divided into domains according to the local composition. The time-independent solution is found for these compositions. Critical fluctuations of statistically correct numbers following Poisson distribution are placed into these areas in every time step. The added small-amplitude noise makes these critical fluctuations either grow or shrink.

In nucleation-growth processes the transformed fraction often follows the Kolmogorov scaling,  $X(t) = 1 - \exp\{-(t/t_0)^p\}$ , where the “Kolmogorov exponent”  $p$  is representative of the mechanism of the phase transformation, and is evaluated from the slope of the plot  $\ln[-\ln(1 - X)]$  vs.  $\ln t$ . In this work  $\phi < 0.5$  is used to define the transformed fraction.

First we apply the phase-field theory to predict nucleation rate in 3D. In the *one-component* Lennard-Jones system, the nucleation rate [15] and all the relevant physical properties are known from molecular dynamics simulations [9]. The radial phase field profiles (Fig. 1a) indicate that the critical fluctuations are diffuse, and do not show bulk crystal properties for undercoolings larger than 14 K. The predicted interfacial free energy (Fig. 1b) increases with temperature. While the phase-field predictions agree with results from computer simulations, those from the classical sharp interface theory differ from the experiments by eight to ten orders of magnitude. Similar results were obtained for the ice-water system (Fig. 2) with input data from [16]. Without adjustable parameters, a quantitative agreement has been achieved with computer simulations [15] and experiment [17], proving the power of the phase-field technique in attacking nucleation problems.

In the case of *binary alloys*, such a rigorous test cannot be performed since the input information available for the crystal-liquid interface is far less reliable. In the nearly ideal Cu–Ni system, the critical undercoolings computed for the realistic range of nucleation rates ( $J = 10^{-4}$  to  $1 \text{ drop}^{-1}\text{s}^{-1}$  for electromagnetically levitated droplets of 6 mm diameter) fall close to the experimental ones [18] (Fig. 3), indicating homogeneous nucleation. This contradicts the heterogeneous mechanism suggested earlier

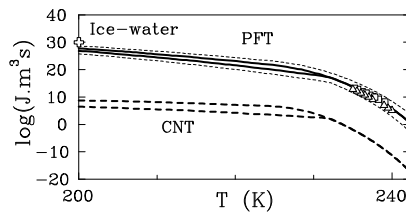


FIG. 2: Nucleation rate vs. temperature in the ice-water system. The experimental results (symbols) are from [17]. The branches below 232 K indicate results obtained with physically reasonable upper and lower estimates for the Gibbs free energy of undercooled water [2]. Notation as in Fig. 1.

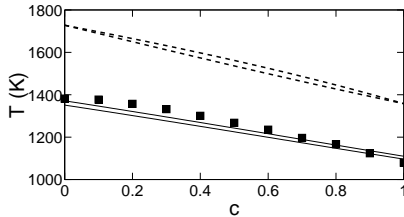


FIG. 3: Nucleation temperature vs. composition that the phase field theory predicts for the nearly ideal Cu–Ni system. Upper and lower solid lines correspond to nucleation rates of  $10^{-4}$  and  $1 \text{ drop}^{-1} \text{s}^{-1}$  for droplets of 6 mm diameter. The experimental data (squares) refer to electromagnetically levitated droplets [18]. The calculated liquidus and solidus lines (dashed) are also shown.

[18] on the basis of Spaepen’s value  $\alpha_{HS} = 0.86$  [19] for the dimensionless interfacial free energy for the hard-sphere system. (For definition of  $\alpha$  see [9].) Recent computer simulations [20] yielded considerably smaller values  $\alpha_{HS} = 0.51$  and  $\alpha_{Ni} = 0.58$  ( $\approx 0.6$  we used), invalidating the earlier conclusion. These findings raise the possibility that homogeneous nucleation is more common in alloys than previously thought.

We turn now to the problem of *soft-impingement* that we investigate in 2D using the properties of Cu–Ni alloys. Owing to the known difficulties of phase field simulations due to different time and length scales of the fields, we used an enhanced interface thickness ( $\delta = 41.6 \text{ nm}$ ), a reduced interfacial free energy ( $\alpha = 0.1$ ), and an increased diffusion coefficient ( $\sim 100 \times D_L$ ). To ensure reasonable statistics and negligible influence of the periodic boundary conditions, the governing equations were solved numerically on a  $7000 \times 7000$  grid under conditions [21] that ensure interfaces consisting of more than ten grid points needed for numerical accuracy.

We begin by comparing three simulations where the particles were nucleated by Method II.: (i) large anisotropy  $s_0 = 0.25$  and small dimensionless nucleation rate  $\tilde{J} = 0.49$  yielding 886 dendritic particles (the first large scale simulation of multiparticle dendritic solidification) [Fig. 4(a)]; (ii)  $s_0 = 0.25$  with large nucleation rate

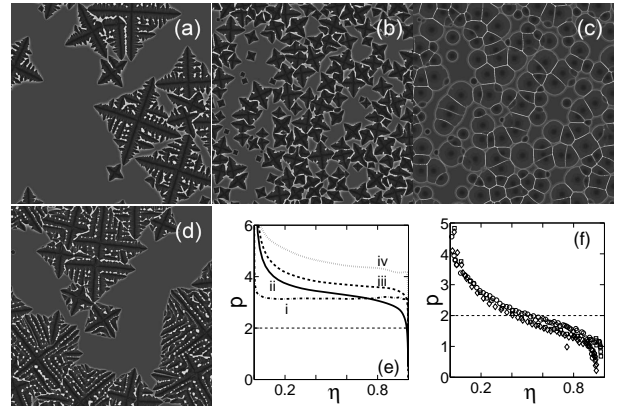


FIG. 4: Soft-impingement in the phase-field theory. (a)–(d)  $1000 \times 1000$  segments of  $7000 \times 7000$  snapshots for the concentration field in cases (i)–(iv), respectively, taken at  $\tilde{t}/\Delta\tilde{t} = 4000, 1500, 1500$ , and  $6000$  (black and white correspond to the solidus and liquidus); (e) Kolmogorov exponent vs. crystalline fraction,  $\eta = X/X_{max}$ , where  $X_{max}$  is the final value of the crystalline fraction; (f) experimental results for the crystallization of amorphous  $\text{Fe}_{73.5}\text{Si}_{17.5}\text{CuNb}_3\text{B}_5$  [4].

$\tilde{J} = 24.5$  (10623 particles) [Fig. 4(b)]; and (iii) isotropic growth with  $\tilde{J} = 24.5$  (10528 particles) [Fig. 4(c)]. The respective Kolmogorov exponents differ from  $p = 2$  that standard references [22] assign for steady-state nucleation and diffusion controlled growth [Fig. 4(d)]. Our prediction for dendritic solidification,  $p \approx 3$ , obeys the relationship  $p = 1 + d$  (constant nucleation and growth rates in  $d$ -dimensions) confirmed experimentally [23], that follows from the steady-state traveling tip solution of the diffusion equation. In cases (ii) and (iii),  $p$  deviates from 2, as the formation of the diffusion layer is preceded by a transient period in which phase field mobility controls growth. This period appears as an effective delay of the diffusion controlled process, yielding an initially enhanced  $p$  that decreases with increasing transformed fraction [4]. This effect is pronounced at large nucleation rates for which the delay is comparable to the solidification time. Indeed, qualitatively similar behavior is observed at the extreme nucleation rates that occur during the formation of nanocrystalline alloys [4].

The introduction of large amplitude noise into the governing equations (Method I.) leads to comparable results. For  $s_0 = 0.25$  with  $\zeta_{\phi,0} = 0.015$ , that yield  $\sim 830$  dendritic particles [case (iv)], more irregular shapes are produced [Fig. 4(d)], and transient nucleation of “induction time”  $\tau/\Delta\tilde{t} \approx 1400$  is observed. The latter leads to further increased  $p$ , that reduces to  $\sim 3$  when replacing  $\tilde{t}$  by  $\tilde{t} - \tau$ . Due to numerical stability problems appearing at large noise amplitudes, Method I. can be applied far from equilibrium, where nucleation occurs in reasonable simulation time and area.

Summarizing, we demonstrated that the present phase field model is able to *quantitatively* describe crystal nu-

cleation in one-component 3D systems. The other predictions, including binary nucleation in 3D and transformation kinetics in 2D, are also consistent with experiment.

This work has been supported by the ESA Prodex Contract No. 14613/00/NL/SFe, by the Hungarian Academy of Sciences under contract Nos. OTKA-T-025139 and T-037323, by the EU grant HPMF-CT-1999-00132, and the ESA MAP Project No. AO-99-101.

A. D. J. Haymet, *J. Chem. Phys.* **114**, 3713 (2001)]. Thus, we adopt  $d_{10-90} \approx d_{10-90,D} = 3\sigma$  [B. B. Laird and A. D. J. Haymet, *Chem. Rev.* **92**, 1819 (1992)], where  $\sigma$  is the length parameter of the LJ potential, while  $d_{10-90} \approx 3(v/N_0)^{1/3}$  is taken for pure substances.

- [10] Eqs. (11) and (12) of [6], after setting  $\nabla T = 0$  and adding  $\xi T_i \mathcal{M} |\nabla \theta| P'(\phi) / (6 \cdot 2^{1/2} \gamma_i \delta_i T)$  to  $H^i$ .
- [11] K. F. Kelton, *Solid State Phys.* **45**, 75 (1991).
- [12] A full evaluation of the field-theoretic prefactor for crystal nucleation where molecular/phase-field mobility is the rate-limiting factor is yet unavailable. The statistical part has been computed for nonlocal interactions in A. Roy, J. M. Rickman, J. D. Gunton, and K. R. Elder, *Phys. Rev. E* **57**, 2610 (1998).
- [13] R. Kobayashi and Y. Giga, *J. Stat. Phys.* **95**, 1187 (1999); R. Kobayashi, J. A. Warren, and W. C. Carter, *Physica D* **140**, 141 (2000).
- [14] A. E. Lobkovsky and J. A. Warren, *Phys. Rev. E* **63**, 051605 (2001); *J. Cryst. Growth* **225**, 282 (2001).
- [15] L. A. Báez and P. Clancy, *J. Chem. Phys.* **102**, 8139 (1995).
- [16] Here  $\gamma = 29.1 \pm 0.8 \text{ mJ/m}^2$  applies [S. C. Hardy, *Philos. Mag.* **35**, 471 (1977)]. Our estimate  $d_{10-90} = 3(v/N_0)^{1/3} \approx 0.96 \text{ nm}$  for the phase field profile falls close to that of the translational order (0.99 nm) [9]. Other relevant properties are from [2].
- [17] P. Taborek, *Phys. Rev. B* **32**, 5902 (1985); G. T. Butorin and V. P. Skripov, *Kristallographiya* **17**, 379 (1972); J. Huang and L. S. Bartell, *J. Phys. Chem.* **99**, 3924 (1995).
- [18] R. Willnecker, D. M. Herlach, and B. Feuerbacher, *Mater. Sci. Eng.* **98**, 85 (1988).
- [19] F. Spaepen and R. B. Meyer, *Scripta Metall.* **10**, 257 (1976).
- [20] R. L. Davidchack and B. B. Laird, *Phys. Rev. Lett.* **85**, 4751 (2000); J. J. Hoyt, M. Asta, and A. Karma, *ibid.* **86**, 5530 (2001).
- [21] The time and spatial steps were  $\Delta \tilde{t} = 4.75 \times 10^{-6}$  and  $\Delta \tilde{x} = 6.25 \times 10^{-3}$ ,  $\xi = 2.1 \times 10^{-4} \text{ cm}$  and  $D_L = 10^{-5} \text{ cm}^2/\text{s}$ . Dimensionless mobilities  $\xi^2 M_\phi / D_L = 0.9$ ,  $\xi M_{\theta,L} \mathcal{M} / D_L = 720$ , and  $\xi M_{\theta,S} \mathcal{M} / D_L = 7.2 \times 10^{-4}$  were applied, while  $D_S = 0$  was taken in the solid. The simulations were performed at 1574 K for  $x = (C_\infty - C_s) / (C_l - C_s) = 0.2$ , where  $C_s = 0.399112$  and  $C_l = 0.466219$  are the solidus and liquidus compositions. White noises of amplitudes  $\zeta_{\phi,0} = 0.0025$ ,  $\zeta_{\nabla c,0} = 0$ , and  $\zeta_{\theta,0} = 0.25$  were used.
- [22] J. W. Christian, *The Theory of Transformations in Metals and Alloys* (Pergamon, Oxford, 1981).
- [23] A. Inoue, D. Kawase, A. P. Tsai, T. Zhang, and T. Masumoto, *Mater. Sci. Eng. A* **178**, 255 (1994).